3D Modelling and Analysis of Parasitic Couplings between Surface-Mount Components of EMI Filters

A. Asmanis[*1], D. Stepins[#2], G. Asmanis[*3], L. Ribickis[*4]
* Institute of Industrial Electronics, Riga Technical University, RTU, Riga, Latvia
[1] ashmanis@inbox.lv, [3] asmanisgundars@inbox.lv, [4] leonids.ribickis@rtu.lv
Institute of Radio Electronics, Riga Technical University, RTU, Riga, Latvia
[2] deniss.stepins@rtu.lv

***Abstract*—In this paper 3D electromagnetic modelling of surface-mount components of EMI filters is presented. Developed models in CST MWS are used to analyze parasitic couplings between surface-mount inductors and surface-mount inductors and capacitors. The couplings are evaluated in terms of transmission coefficients. Modelling results are then verified experimentally over wide frequency range. The models can be fairly useful to predict the mutual couplings in the frequency range from several MHz to several tens of MHz.**

Keywords—capacitors; inductors; EMI filters; electromagnetic coupling; modelling.

I. INTRODUCTION

With an ever increasing demand for miniaturization of power electronic converters, electromagnetic interference (EMI) filters have become an inalienable part of them. Modern EMI filters should combine low volume and weight along with high EMI attenuation [1], [2]. Traditional EMI filters usually have through-hole technology (THT) components which are quite bulky and have rather degraded performance at high frequencies due to long leads. Meanwhile surface-mount technology (SMT) components have noticeably smaller dimensions and lower parasitics than THT components. As switching frequencies of power electronic converters are increasing rapidly (mainly because of rapid development of GaN devices) [3], EMI filters with SMT components become popular. EMI filters are used not only to reduce conducted EMI in power electronic converters, but also to reduce EMI in data lines, motherboards, etc.

In order to reduce EMI filter size, filter components (capacitors and inductors) should be placed very close to each other. However EMI filter performance can degrade significantly at high frequencies (in MHz region) due to increased parasitic electromagnetic couplings between the components [4] – [7].

For prediction of EMI filter performance considering the parasitic couplings between the filter components, it is useful to use 3D electromagnetic modelling software such as CST MWS [8]. Although much research has been carried out over the last decade to model THT components and parasitic couplings between them using 3D electromagnetic modelling tools [8] – [11], there is only one paper [12] dedicated to modelling SMT capacitors and mutual couplings between them.

This paper is the continuation of the study presented in [12]. In this paper 3D models of SMT inductors are developed and parasitic couplings between SMT inductors and SMT inductors and capacitors are analyzed in details over wide frequency range using both 3D electromagnetic modelling software CST MWS and experimentally using a vector network analyzer (VNA) Rohde & Schwarz ZVRE.

II. 3D SMT INDUCTOR MODELS

3D models of SMT capacitors were presented in [12]. In this chapter 3D models of SMT inductors are described and validated experimentally.

Miniature SMT inductors in terms of their internal structure can be divided into three main categories: 1) wire-wound SMT inductors; 2) multi-layer SMT inductors and 3) film SMT inductors [13]. One of the specific types of SMT inductors is SMT ferrite bead. To reduce EMI noise at inputs and outputs of power supplies, SMT ferrite beads are often used. SMT ferrite beads in terms of internal structure are somewhat similar to multi-layer SMT inductors [14] - they have multi-layer conductor. The main difference between them is that SMT ferrite beads have conductors created between many ferrite sheets layers [14]. Ferrite exhibits high energy losses at high frequencies to better suppress EMI.

In this paper 3D models of three different SMT inductors (WE 742792141, WE 744066151, WE 7447709471) made by Wurth Electronics Inc. are developed in CST MWS. Inductor WE 742792141 is a ferrite bead having multi-layer structure, but inductors WE 744066151 and WE 7447709471 are wire-wound shielded inductors with ferrite core [15].

3D models of the wire-wound inductors developed in CST MWS are shown in Fig.1 and Fig.2. Since number of turns, diameter of winding wire and ferrite core parameters (core dimensions, ferrite complex permeability, complex permittivity and resistivity as functions of frequency) were known for us, they were taken into account in the models. The winding wires do not have insulation in the models, because, firstly, we did not know the insulation parameters (e.g.

This work has been supported by the Latvian National Research Programme "LATENERGI".

thickness) accurately, and secondly, omitting insulation in the models helps in reducing modelling time noticeably.

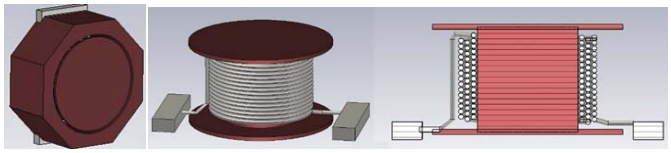

(a) (b) (c)

Fig.1. 3D models of SMT wire-wound inductor WE 744066151 created in CST MWS: (a) 3D model with a shield; (b) 3D model without the shield; (c) cross section view of the 3D model.

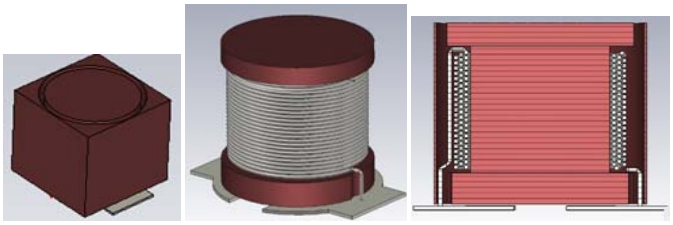

(a) (b) (c)

Fig.2. 3D models of SMT wire-wound inductor WE 7447709471 created in CST MWS: (a) 3D model with a shield; (b) 3D model without the shield; (c) cross section view of the 3D model.

Since Wurth Electronics does not disclose information about ferrite complex permeability, complex permittivity and resistivity over wide range of frequencies for the ferrite beads (such as WE 742792141), we created 3D model of the ferrite bead using a parametric surface which was described by S (scattering) parameters obtained experimentally for the ferrite bead using the VNA. The model is shown in Fig.3 with experimental S parameters magnitudes as functions of frequency. Unfortunately, this simple model of the ferrite bead does not give us a possibility to estimate the mutual couplings between inductive components accurately. This is why more complex 3D model of the ferrite bead was developed in CST MWS as shown in Fig.4. The model has accurate multi-layer winding structure with single parametric surface with integrated S parameters obtained experimentally.

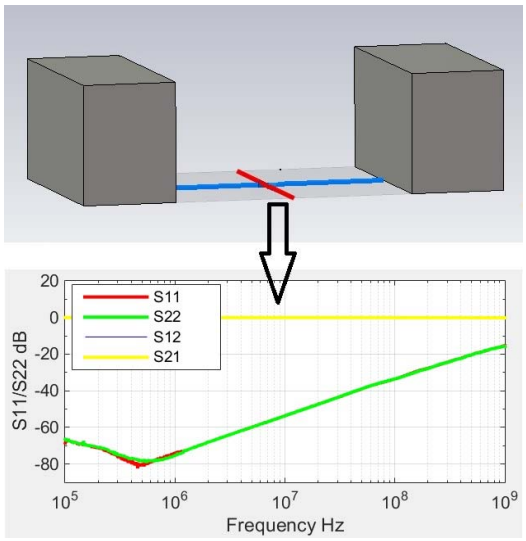

Fig.3. CST MWS 3D model of the ferrite bead described by single parametric surface with integrated S parameters (obtained experimentally).

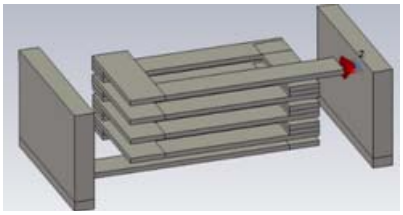

Fig.4. More accurate 3D model of the ferrite bead having multi-layer winding structure with single parametric surface with integrated S parameters obtained experimentally. Note: this model does not have ferrite sheet layers between the winding layers.

III. Experimental Validation of the Inductor Models

In order to validate developed models in CST MWS, PCBs with the inductors and SMA connectors were created and measurements using series-through technique [16] with VNA ZVRE were done. In order to extract impedances of the inductors de-embedding of the inductor parameters was performed using the procedure proposed in [16]. A picture of SMT ferrite bead under measurements and PCB with SMA connectors is shown in Fig.5. Comparison of the measurement and modelling results is depicted in Fig.6 for three different SMT inductors.

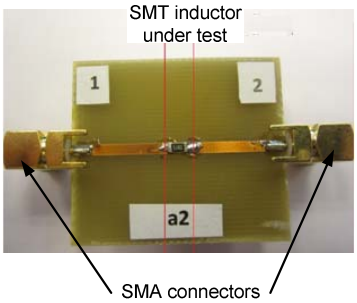

Fig.5. A picture of SMT inductor (WE 742792141) under measurements with PCB and SMA connectors.

Rather good agreement is achieved between the modelling and the experimental results for SMT ferrite bead over wide range of frequencies. This good agreement can be explained by the fact that the model of the SMT ferrite bead has multi-layer winding structure with single parametric surface with integrated S parameters obtained experimentally. It should be noted that even if there is good agreement between experimental and modelled impedances of the ferrite bead, it does not mean that this model will allow us to accurately estimate parasitic mutual couplings between filter components. This is due to the fact that the model shown in Fig.4 does not have ferrite sheet layers between the conductor layers.

For surface mount technology wire-wound inductor (WE 744066151) there is also good agreement between experimental and modelled impedances in the range of frequencies between 100 kHz and 4 MHz as shown in Fig.6. However in the range of frequencies close to the inductor self-resonant frequency and above it there is noticeable disagreement between the results. This can be explained as follows: firstly, we purposely removed thin insulation layer from the winding wire in the model (Fig.1) due to the reasons described in the second chapter, and secondly, we did not

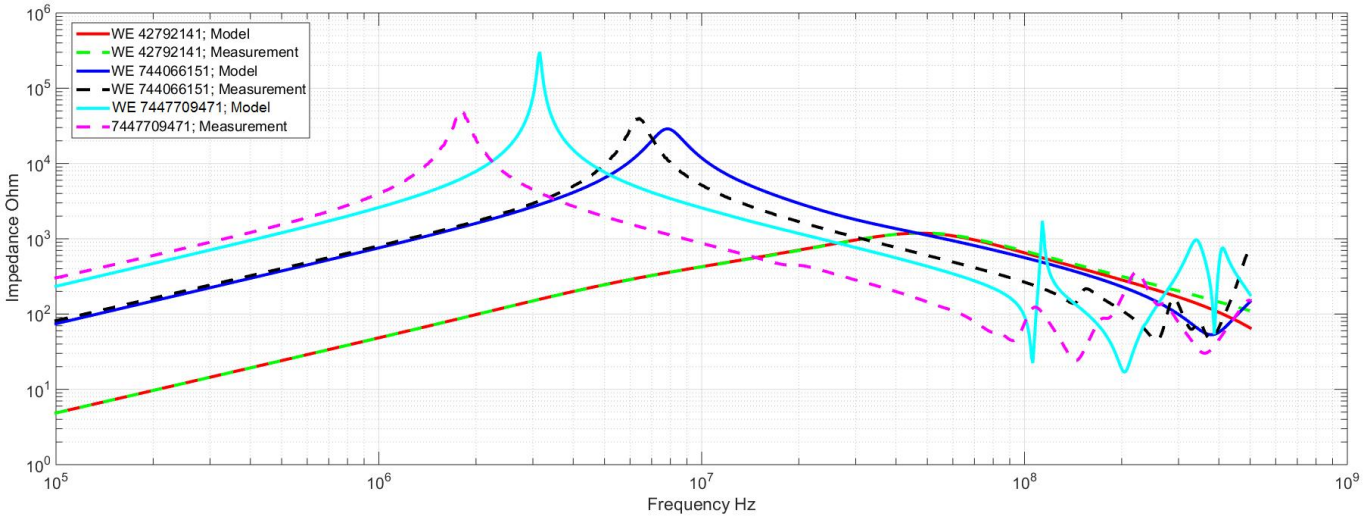

Fig. 6. Impedance versus frequency for different inductors.

know accurately the spacing between the winding wire's turns (apparently the spacing in the model was higher than that in real life). As a result of this parasitic equivalent parallel capacitance of the inductor model was lower than in real life and consequently there is noticeable disagreement between the impedances for frequencies close to and above the self-resonant frequency of the SMT wire-wound inductor as it can be seen in Fig. 6. The same explanation of disagreement between modelled and measured impedances for frequencies close to or above the self-resonant frequency is applicable for the SMT inductor WE 7447709471.

IV. Study of the Parasitic Couplings

In this chapter parasitic mutual couplings between various SMT inductors and SMT inductors and capacitors are evaluated in terms of transmission coefficients S_{21} using developed 3D models of inductors and capacitors (with PCB and SMA connectors) and experimentally. For S_{21} measurements VNA ZVRE is used.

A. Parasitic couplings between SMT inductors

In order to study parasitic couplings between SMT inductors, S_{21} was measured and modelled for 5 different types of PCBs: a) type d1 (Fig. 7(a)) to study mutual couplings between two SMT ferrite beads (WE 742792141); b) type d2 (Fig. 7(b)) to study mutual couplings between SMT wire-wound inductor (WE 744066151) and SMT ferrite bead (WE 742792141); c) type d3 (Fig. 7(c)) to study mutual couplings between two SMT wire-wound inductors (WE 744066151); d) type d4 (Fig. 7(d)) to study mutual couplings between two SMT wire-wound inductors (WE 7447709471); e) type d5 (Fig. 7(e)) to study mutual couplings between SMT wire-wound inductor (WE 7447709471) and SMT ferrite bead (WE 742792141). For each type of PCB there were created three similar PCBs with different distances (1 mm, 3 mm and 5 mm) between the inductors.

Measurement and modelling results for type d1 PCB with different distances between the components are shown in Fig.8. As it can be seen measurement and modelling results agree quite well for frequencies above 10 MHz: the maximum difference between the results is below 2 dB. However there is rather high difference (more than 10 dB) between the measurement and modelling results for frequencies below 3MHz when the distance between the components is 1 mm or 3 mm. This can be explained by the fact that in the SMT ferrite 3D model (Fig.4) ferrite layer sheets (placed between winding layers) are not used. At low frequencies (up to several MHz) ferrite has quite high real part of complex permeability and this is why not taking into account the ferrite parameters in the model leads to poor ability to estimate the mutual couplings accurately. However for frequencies exceeding 10 MHz real part of magnetic permeability of ferrite material starts to decrease significantly. As the result the ferrite has almost no influence on the mutual couplings and accuracy of the modelling results is rather good.

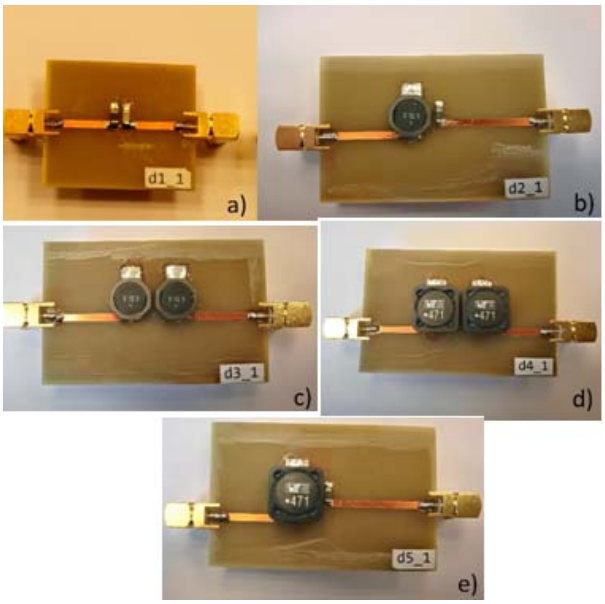

Fig.7. Pictures of different-type experimental PCBs with soldered SMT inductors when distance between them is 1 mm.

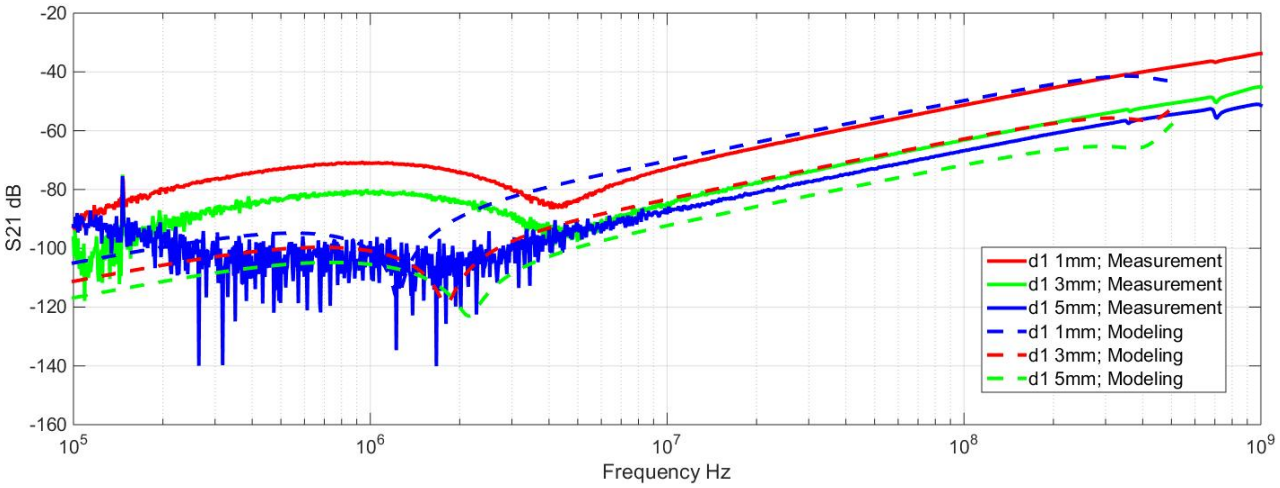

Fig. 8. Magnitude of S_{21} as a function of frequency PCB type d_1.

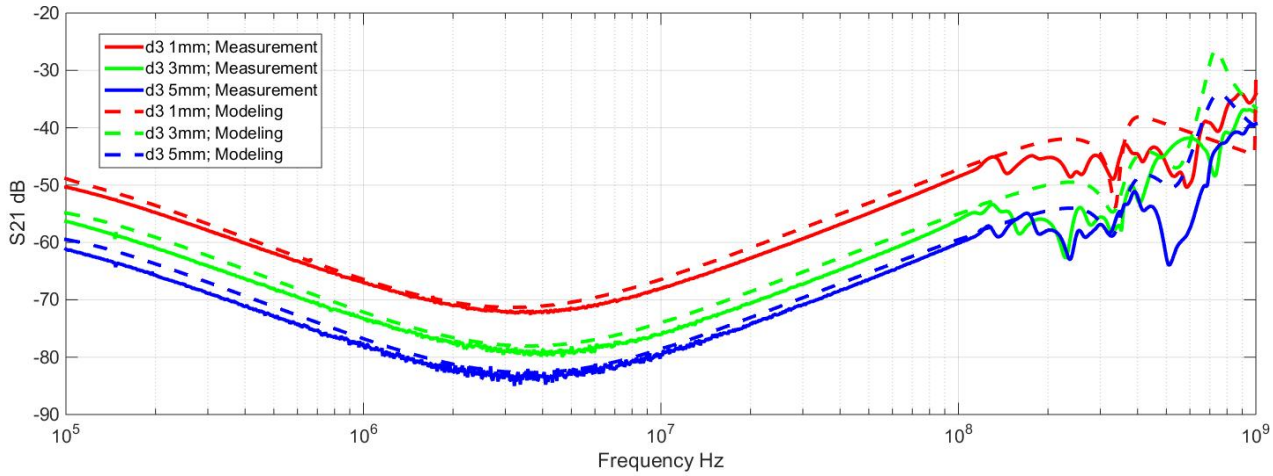

Fig. 9. Magnitude of S_{21} as a function of frequency PCB type d_3.

Measurement and modelling results for type d3 PCB with different distances between the components are shown in Fig.9. The measurement results fit the modelling results quite well in the range of frequencies between 100 kHz and 100 MHz. However for frequencies above 200 MHz there is quite high disagreement between the results, probably because ferrite parameters were not well defined for that frequencies and division of the 3D model to smaller finite elements should be performed.

Rather good agreement between the modelling and experimental results (Fig. 10) is also achieved for type d4 PCB in the range of frequencies between 100 kHz and 10 MHz. However for frequencies above 100 MHz there is quite high disagreement between the results. The reasons for this are similar to that for d3 PCB.

The modelling results (Fig. 11 and Fig. 12) fit quite well the experimental results for PCB type d2 and PCB type d5 in the range of frequencies between 3 MHz and 100 MHz. Rather high discrepancy between the results takes place for PCB type d2 for frequencies below 2 MHz. This can be explained by the fact that the ferrite bead model does not into account ferrite sheet layers between the winding layers. For lower frequencies ferrites have quite high real part of complex magnetic permeability and as a result they have major influence on the couplings.

As it can be seen from the results the mutual couplings between the inductors tend to increase as frequency increases. This can be explained by electromagnetic induction: the higher the rate of change of magnetic flux (created by the current flowing through the first inductor loop) is, the higher electromotive force induced in the second inductor loop is.

B. Parasitic couplings between SMT inductors and capacitors

In order to study parasitic couplings between SMT inductors and capacitors, transmission coefficient S_{21} was measured using VNA and modelled for different distances between 4.7 nF SMT capacitor and wire-wound SMT inductor WE 744066151. Model of SMT capacitor is taken from our previously published paper [12]. Experimental and measurement results are compared in Fig. 13. As it can be seen the modelling results fit experimental results very well for range of frequencies between 100 kHz and 40 MHz. For

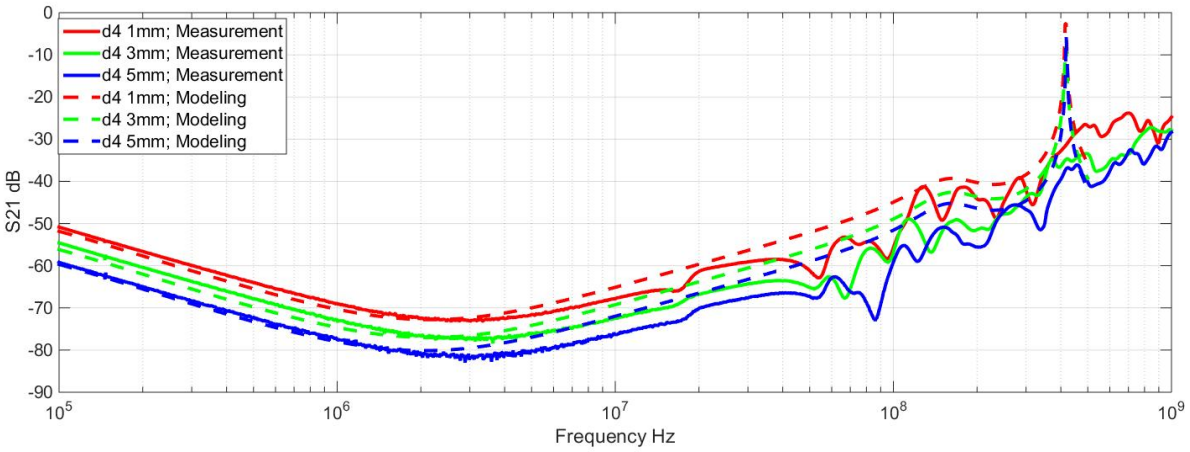

Fig. 10. Magnitude of S_{21} as a function of frequency PCB type d_4.

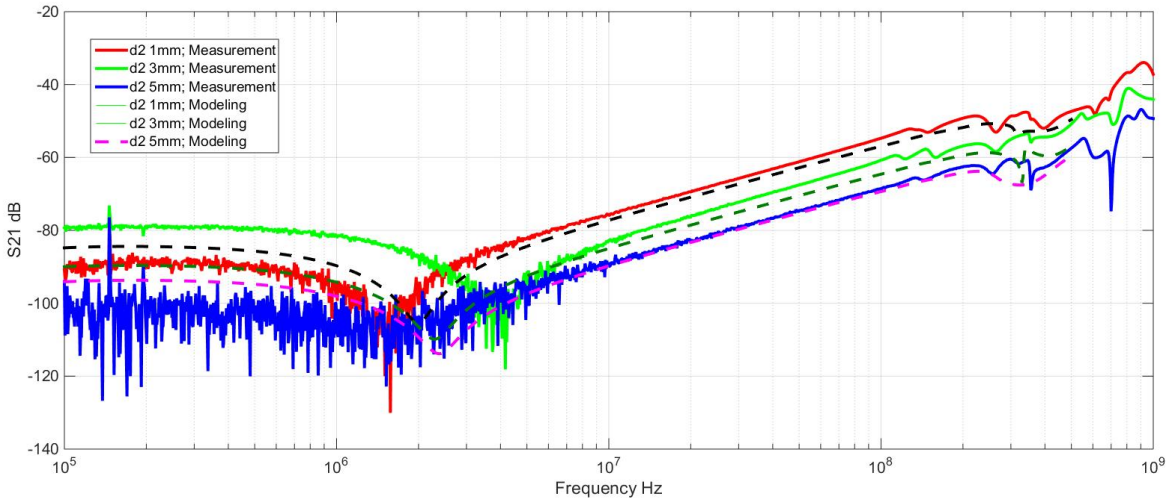

Fig. 11. Magnitude of S_{21} as a function of frequency PCB type d_2.

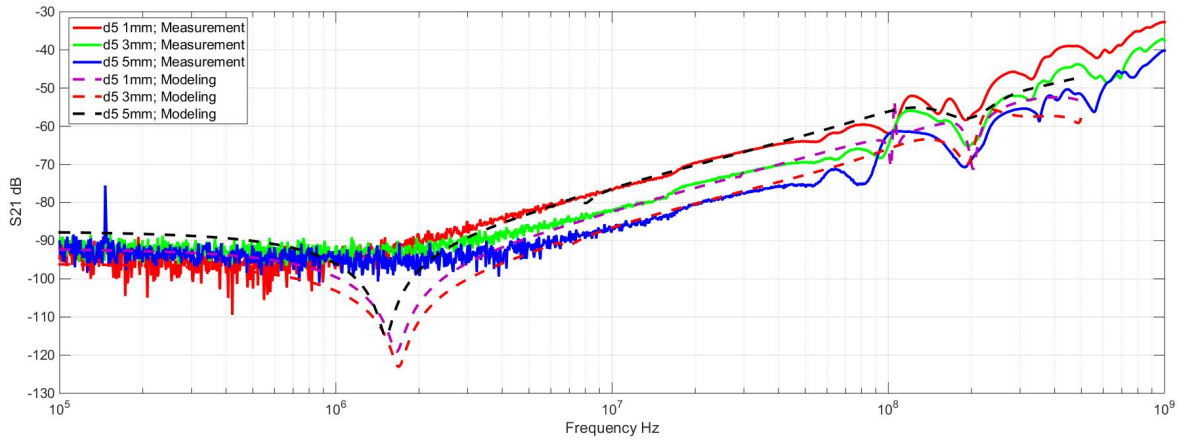

Fig. 12. Magnitude of S_{21} as a function of frequency PCB type d_5.

frequencies above 100 MHz a discrepancy between the results is high. Therefore further work should be dedicated to improve accuracy of inductor and capacitor models.

V. Conclusions

Since conductor layer thickness is much lower than SMT inductor dimensions, then for accurate 3D modelling of

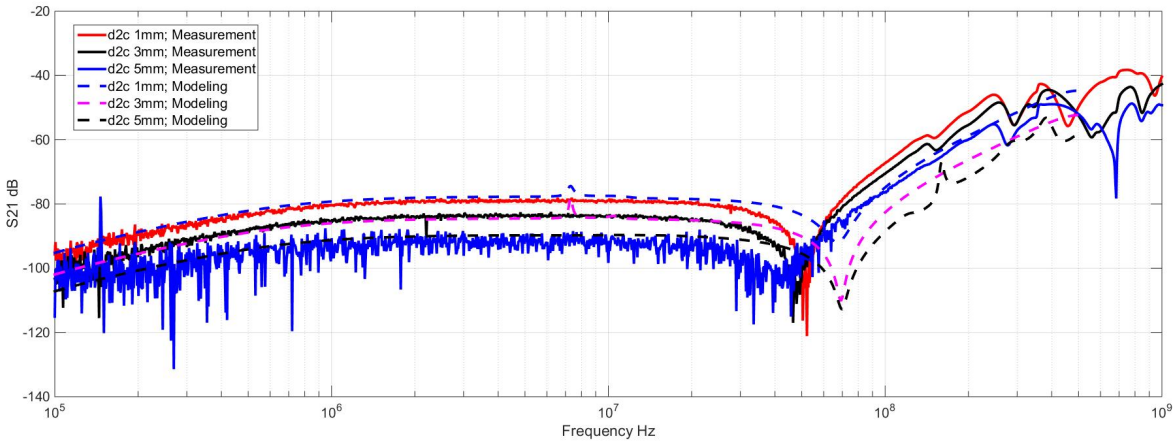

Fig. 13. Magnitude of S_{21} as a function of frequency for PCB with SMT capacitor and inductor.

inductors it is necessary to divide the model into many finite elements (which number can exceed 10^6). Accurate 3D models of SMT inductors taking into account complex internal structure of them are possible to create in CST MWS, but it will require a lot of computational memory and computer resources. Modelling of such complex 3D models will be time-consuming task. This is why simpler 3D models of the inductors are developed in this paper.

These models can give us a possibility to predict the mutual couplings with fairly good accuracy from several MHz to several tens of MHz. For frequencies above several hundreds of MHz accuracy of prediction of the mutual couplings is quite poor. The accuracy of the predictions will be improved if we know winding wire insulation parameters and turns spacing accurately, and if division of the 3D model to much smaller finite elements is performed. However in this case computational time and memory requirements will significantly increase. So there is trade-off between accuracy of predictions and consumed time and resources. Increase in accuracy of the models without significant increase in consumed time and resources will be dedicated to the further research.

REFERENCES

[1] Y. Murata, K. Takahashi, T. Kanamoto and M. Kubota "Analysis of Parasitic Couplings in EMI Filters and Coupling Reduction Methods," IEEE Transactions on Electromagnetic Compatibility, April 24, 2017, pp. 1880 - 1886.

[2] R. Wang, H. F. Blanchette, M. Mu, D. Boroyevich and P. Mattavelli. "Influence of High-Frequency Near-Field Coupling Between Magnetic Components on EMI Filter Design," IEEE Transactions on Power Electronics, October 2013, pp. 4568 – 4579.

[3] Yilin Sha, et al. "Research of active EMI filter for Gallium Nitride based high frequency resonant converter," Proc. of the 2016 Asia-Pacific International Symposium on Electromagnetic Compatibility (APEMC), 2016, pp. 491-494.

[4] G. Asmanis, D. Stepins, A. Asmanis, and L. Ribickis, "Capacitors mutual inductance modeling and reduction," Proc. of the International Symposium on Electromagnetic Compatibility (EMC Europe 2014), Sweden, Gothenburg, 1-4 September, 2014, pp.1176-1181.

[5] N. Moonen, F. Buesink, and F. Leferink, "Enhanced circuit simulation using mutual coupling parameters obtained via 3D field extraction," in Asia-Pacific International Symposium on Electromagnetic Compatibility & Signal Integrity (APEMC), Shenzhen, China, May 2016, pp. 576-580.

[6] M. Stojanovic, et al. "Modified Kron's Method (MKME) for EMC optimization, applied to an EMC filter". Proc. of the 2016 Asia-Pacific International Symposium on Electromagnetic Compatibility (APEMC), 2016, pp. 782-784.

[7] Shuo Wang, F.C. Lee, W.G. Odendaal, and J.D. van Wyk, "Improvement of EMI Filter Performance with Parasitic Coupling Cancellation," in Power Electronics Specialists Conference, Recife, 2005, pp. 1780 - 1786.

[8] G. Asmanis, L. Ribickis, D. Stepins and A. Asmanis, "Differential mode Π-type EMI filter modeling using CST MWS," Proc. of 56th International Scientific Conference on Power and Electrical Engineering of Riga Technical University (RTUCON 2015), Latvia, Riga, October 14, 2015, pp. 1 - 5.

[9] G. Asmanis, D. Stepins, L. Ribickis, and A. Asmanis, "Modeling of Mutual Coupling between Inductors," Proc. of IEEE Symposium on Electromagnetic Compatibility and Signal Integrity, USA, Santa Clara, 15-20 March, 2015, pp.294-299.

[10] I. F. Kovacevic, T. Friedli, A. M. Musing, and J. W. Kolar, "3-D electromagnetic modeling of parasitics and mutual coupling in EMI filters," IEEE Transactions on Power Electronics, vol. 29, no. 1, pp. 135-149, Jan. 2014.

[11] I. Manushyn, and G. Griepentrog, "Finite element method based electromagnetic modeling of three-phase EMI filters," Proc. of IEEE Annual Southern Power Electronics Conference (SPEC 2016), December 2016, pp. 1-6.

[12] A. Asmanis, D. Stepins, A. Dzenis, and G. Asmanis, "3D Modeling of Surface-Mount Capacitors and Mutual Couplings between Them," Proc. of the International Symposium on Electromagnetic Compatibility (EMC Europe 2017), France, Angers, 4-8 September, 2017, pp.1-6.

[13] https://www.murata.com/products/inductor/chip/feature/rf

[14] Basics of Noise Countermeasures [Lesson 4] Chip ferrite beads: https://www.murata.com/products/emiconfun/emc/2011/06/14/en-20110614-p1

[15] https://katalog.we-online.de/pbs/datasheet/7447709471.pdf

[16] D. Stepins, G. Asmanis, A. Asmanis, "Measuring Capacitor Parameters Using Vector Network Analyzers," Electronics, vol.18, no.1, pp.29-38, June 2014.

This is a post-print of a paper published in Proceedings of the 2018 IEEE International Symposium on Electromagnetic Compatibility and 2018 IEEE Asia-Pacific Symposium on Electromagnetic Compatibility (EMC/APEMC 2018), Suntec City, Singapore, 14-18 May 2018 and is subject to IEEE copyright. https://doi.org/10.1109/ISEMC.2018.8393828
ISBN 978-1-5090-3955-5 ; e-ISBN 978-1-5090-5997-3.